Journal of Vertebrate Paleontology
Publication details, including instructions for authors and subscription information:
http://www.tandfonline.com/loi/ujvp20

Bone histology confirms determinate growth and small body size in the noasaurid theropod Masiakasaurus knopfleri

Andrew H. Lee [a] & Patrick M. O'Connor [b]

[a] Department of Anatomy , Midwestern University , Glendale , Arizona , 85308 , U.S.A.

[b] Department of Biomedical Sciences , Ohio University Heritage College of Osteopathic Medicine , Athens , Ohio , 45701 , U.S.A.

Published online: 25 Jun 2013.

To cite this article: Andrew H. Lee & Patrick M. O'Connor (2013): Bone histology confirms determinate growth and small body size in the noasaurid theropod Masiakasaurus knopfleri , Journal of Vertebrate Paleontology, 33:4, 865-876

To link to this article: http://dx.doi.org/10.1080/02724634.2013.743898

Journal of Vertebrate Paleontology 33(4):865–876, July 2013

ARTICLE

BONE HISTOLOGY CONFIRMS DETERMINATE GROWTH AND SMALL BODY SIZE IN THE NOASAURID THEROPOD *MASIAKASAURUS KNOPFLERI*

ANDREW H. LEE*[,1] and PATRICK M. O'CONNOR[2]
[1]Department of Anatomy, Midwestern University, Glendale, Arizona 85308, U.S.A., alee712@gmail.com;
[2]Department of Biomedical Sciences, Ohio University Heritage College of Osteopathic Medicine, Athens, Ohio 45701, U.S.A., oconnorp@ohio.edu

ABSTRACT—Noasauridae is a clade of ceratosaurian theropods that evolved small body size independently of other non-avian theropods. The best-preserved and most complete noasaurid is *Masiakasaurus knopfleri* from the Maastrichtian-aged Maevarano Formation in Madagascar. An abundance of skeletal material from several individuals spanning a wide range of ontogeny makes *Masiakasaurus* an ideal candidate for the analysis of growth. We histologically sampled a growth series of elements consisting of four femora and three tibiae. Bright-field and circularly polarized light microscopy were used to distinguish between slowly and rapidly growing forms of bone. To simultaneously estimate age at death and reconstruct growth trajectories, we measured the perimeters of growth lines in each specimen and fitted models to these data using a novel application of mixed-effects regression. Our histological results show an external fundamental system in the largest tibial specimen and confirm that *Masiakasaurus* grew determinately, matured at small body size, and is not the juvenile form of a larger-bodied theropod. Parallel-fibered bone is unusually prominent and suggests relatively slow growth. Moreover, our quantitative analysis shows that the average individual took about 8–10 years to get to the size of a large dog. Although *Masiakasaurus* grew 40% faster than crocodylians, it grew about 40% slower than comparably sized non-avian theropods. Slowed growth may have evolved as a means to minimize structural and maintenance costs while living in a semiarid and seasonally stressful environment. Dimorphism does not appear related to asymptotic size or growth rate but seems to reflect the degree of skeletal maturity.

SUPPLEMENTAL DATA—Supplemental materials are available for this article for free at www.tandfonline.com/UJVP

INTRODUCTION

Abelisauroid ceratosaurs were once the dominant terrestrial predators across much of Late Cretaceous Gondwana, particularly South America, India, and Madagascar where their remains are the most commonly recovered theropod fossils (Tykoski and Rowe, 2004; Carrano and Sampson, 2008). Despite this apparent diversity, incomplete or poor preservation in many abelisauroid taxa limits phylogenetic resolution within the group. The recent inclusion of new fossils in phylogenetic analyses has clarified the taxonomic compositions of Abelisauroidea and its two major subclades, Abelisauridae and Noasauridae. Nevertheless, the general paucity of complete specimens continues to obfuscate both relationships within the subclades and the identification of evolutionary trends, particularly the reduction in size among noasaurids (Carrano and Sampson, 2008; Carrano et al., 2011).

The best-preserved and most complete noasaurid ceratosaur is *Masiakasaurus knopfleri* (Sampson et al., 2001; Carrano and Sampson, 2008; Carrano et al., 2011). Its remains are known exclusively from the Late Cretaceous (Maastrichtian) Maevarano Formation (Sampson et al., 2001) exposed in the Mahajanga Basin of northwestern Madagascar. To date, the hypodigm of *Masiakasaurus* consists of hundreds of isolated skeletal elements representing many individuals between ~1.4 and 2.3 m in body length (Carrano et al., 2002, 2011). The broad range in body size (and presumed ontogeny) exhibited by *Masiakasaurus* (Carrano et al., 2011) and the abundance of provenance-constrained recovered specimens are ideal for histological analyses aimed at characterizing skeletal growth and maturity. Such analyses can test whether the largest specimens derive from individuals that were fully grown, thereby providing a developmental criterion to support *Masiakasaurus* as a small-bodied taxon. In addition, external measurements and certain discrete features (e.g., presence or absence of muscle scars) thought to represent sexual-dimorphic characteristics of whole skeletal elements (Carrano et al., 2002, 2011) can now be viewed in conjunction with histological data that may record differential growth profiles in the two morphs. Finally, the general paucity of ontogenetic sampling in basal neotheropods has severely limited the study of growth to four taxa: the coelophysoid '*Syntarsus*' (cf. *Coelophysis*; Yates, 2005) *rhodesiensis*, the basal ceratosaur *Limusaurus inextricabilis*, and the allosauroids *Allosaurus fragilis* and *Acrocanthosaurus atokensis*. Histological data from 13 femora of *Coelophysis* and a fibula of *Limusaurus* suggest that these small-bodied taxa took 4–6 years to reach full size (Chinsamy, 1990; Xu et al., 2009). In contrast, data from 20 long bones of *Allosaurus* and six long bones of *Acrocanthosaurus* reveal that these large-bodied taxa grew for approximately 18–28 years (Bybee et al., 2006; Lee and Werning, 2008; D'Emic et al., 2012) and that sexual maturity, at least for *Allosaurus*, occurred by the relatively young age of 10 years (Lee and Werning, 2008). The well-preserved and relatively abundant materials of *Masiakasaurus* represent a unique opportunity to characterize the growth of another small-bodied basal neotheropod, thereby providing a comparative reference point for non-avian theropods more generally.

MATERIALS AND METHODS

Sectioning and Imaging of Specimens

Specimen Selection and Sectioning—Hind limb elements of *Masiakasaurus* span a wide size and presumably ontogenetic

*Corresponding author.

TABLE 1. Mid-diaphyseal circumference (mm) and bone length (mm) of specimens, type of muscle scarring, circumferences of LAGs (mm), and estimated ages at death (years).

Element	Specimen	Scars	Circumference/ Length	LAG circumference	Est. age[1]	Est. age[2]	Est. age[3]	Est. age[4]	Est. age[5]	Est. age[6]	Est. age[7]
Femur	FMNH PR 2153	w	33.6 / 130*	27.0*	1est	2est	2est	3est	6est	8est	5est
	FMNH PR 2150	w	48.4 / 160*	32.2*, 39.3*, 44.5*	4	4	5	6	7	9	8
	FMNH PR 2215	w	53.0 / 180.0	40.8*, 46.0, 49.5, 52.4	6	7	7	8	10	12	11
	FMNH PR 2123	r	62.9 / 202.5	44.6*, 48.9, 54.5, 58.4, 61.3, 62.2	9	10	10	12	16	20	14
Tibia	FMNH PR 2152	w	26.2 / 110*	21.3	1est	1est	2est	3est	5est	7est	4est
	UA 8710	w	37.1 / 140*	27.3*, 30.7, 33.3, 36.6	7	8	9	11	14	16	9
	UA 8685	r	57.1 / 205.4	36.1*, 45.6, 51.8, 54.0, 55.4, 56.3, 56.7	7	7	8	9	10	12	16

Abbreviations: **1**, monomolecular; **2**, von Bertalanffy; **3**, Gompertz; **4**, logistic; **5**, extreme value function; **6**, innominate; **7**, linear; **est**, estimated from mean curve; **r**, robust; **w**, weak. *Reconstructed.

range. Femoral and tibial mid-diaphyseal circumferences range from 35 to 65 and 28 to 53 mm, respectively (Carrano et al., 2002, 2011). We selected elements (Table 1) from the lower, middle, and upper portions of these ranges and assembled a growth series of femora and tibiae consisting of four and three specimens, respectively. Prior to histological sampling, casts and photographs of the specimens were prepared. To standardize comparisons within each series of hind limb elements, we marked positions for our desired sections at 60% of the proximodistal length in femora and midway along the length in tibiae where both elements are the narrowest and presumably preserve the longest growth record (Fig. 1). Transverse cuts were made ~5 mm proximal and distal to the desired level of section using a rotary tool (Dremel). The mid-diaphyseal blocks were vacuum embedded in polyester resin (Interplastic Corporation Silmar S-40). Transverse thick sections were cut using a low-speed wafering saw (Buehler Isomet 1000), mounted to glass slides with two-ton epoxy (Devcon S-31), and manually ground to optical translucency on a grinding wheel (Buehler Ecomet 3000).

Polarized Light Microscopy—Completed sections were viewed under transmitted circularly polarized light to visually assess matrix organization (e.g., bulk optical luminosity of parallel-fibered vs. mosaic-like luminosity of woven-fibered matrix) as well as non-polarized light to create full-section montages. We used circular polarization instead of crossed linear polarization because the latter mode blocks light parallel to the transmission axes of the linear polarizers, thereby introducing optical extinction artifacts (the black 'Maltese Cross' effect; Bromage et al., 2003). Similar extinction artifacts (albeit magenta in color) occur when coupling crossed linear polarization with a full-wave (also known as first-order, gypsum, lambda, or red-tint) retardation plate (elliptical polarization). In contrast, circular polarization eliminates the artifacts, which are easily misinterpreted as longitudinally or randomly oriented bone collagen, and gives correct information about fiber orientation regardless of how the slide is rotated (Bromage et al., 2003). We did, however, use elliptical polarization to test for the preservation of collagen, which has a characteristic positive elongation.

Creating Virtual Histology Slides—To create full-section montages, we first captured hundreds of overlapping images using transmitted non-polarized light microscopy (Nikon Optiphot-2; 4× plan achromat objective: numerical aperture = 0.1, resolution ≈ 3.4 μm) following the methodology of Bybee et al. (2006). Reassembly of the overlapping images was performed by automated image-stitching software (Kolor Autopano Pro). However, the resulting full-section montages were distorted because the software was designed for panoramic photography, which involves mapping images onto a sphere (spherical projection). Instead, we wanted the software to map images along a two-dimensional (2D) array like a flatbed scanner (orthographic projection). To emulate orthographic projection, we changed the focal length values embedded in each image to 1,000,000 mm or infinity (Phil Harvey, ExifTool). The resulting undistorted montages were sharpened by applying the 'Smart sharpen' filter in Adobe Photoshop. Montages were gigantic and unwieldy ranging between 164 megapixels to 1.4 gigapixels. In order to obtain manageable file sizes with minimal loss of information (Nyquist threshold < 1.4 μm per pixel), images were reduced in size to 20–90 megapixels with a resolution between 1.3 and 2.5 μm per pixel. All montages are freely accessible as interactive virtual microscope slides at http://paleohistology.appspot.com.

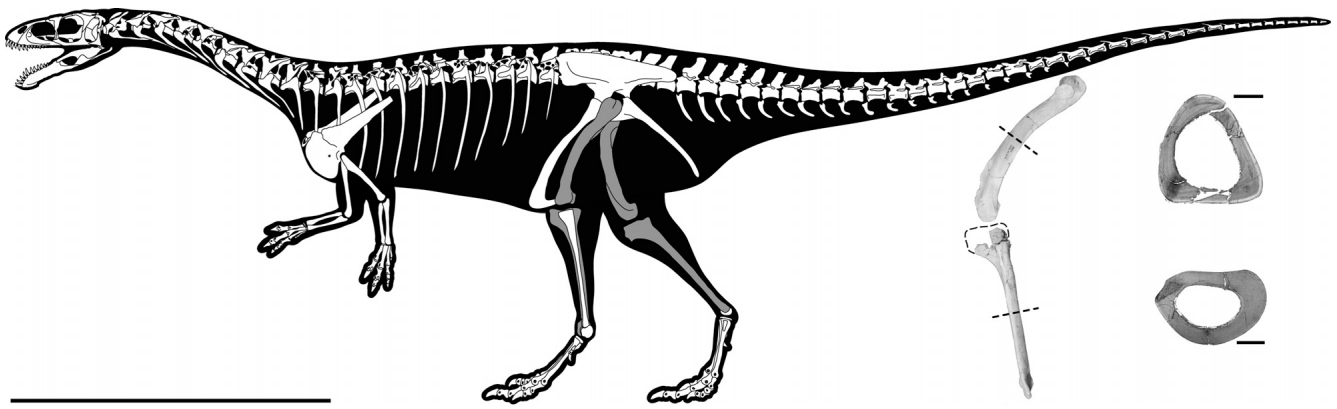

FIGURE 1. Reconstruction of *Masiakasaurus knopfleri* in left lateral view to illustrate elements sampled (gray shading), location of sectioning within respective elements, and representative histological images used in this study. Scale bar equals 0.5 m for the skeletal reconstruction and 5 mm for the histological sections. Skeletal reconstruction courtesy of M. Carrano.

Institutional Abbreviations—**FMNH PR**, Field Museum of Natural History, Chicago, U.S.A.; **UA**, Université d'Antananarivo, Antananarivo, Madagascar.

Growth Curve Reconstruction

Cortical Growth Marks—Periosteal bone growth is measurable because the cortical bone of most tetrapods preserves temporal markers called lines of arrested growth (LAGs). Such markers occur broadly among extinct tetrapods (e.g., de Ricqlès et al., 2004; Turvey et al., 2005; Sander and Andrassy, 2006) as well as their extant relatives in which each LAG marks the period of decreased growth rate or dormancy in an annual growth cycle (e.g., Morris, 1970; Frylestam and Schantz, 1977; Hemelaar and Van Gelder, 1980; Hutton, 1986; Castanet, 1994; Castanet et al., 2004; de Ricqlès et al., 2004; Köhler et al., 2012). Therefore, LAGs are useful not only for age estimation but also for tracking changes in the annual rate of periosteal bone growth.

Reconstructing Eroded Growth Marks—In each sectional montage, we applied the method first introduced by Bybee et al. (2006) to digitally trace LAGs (Adobe Illustrator), measure their circumferences (NIH ImageJ), and compile LAG circumferences in sequential order (Table 1). Ideally, the incremental sequence of LAGs in a bone represents the entire growth record of an individual. However, complete preservation of the record is rare because (1) death occurred prior to the completion of growth or (2) expansion of the medullary cavity obliterated the early growth record, effectively leaving only a segment of the growth trajectory (Fig. 2). Because LAG sequences that lack the early growth record underestimate age at death and bias interpretations of growth (e.g., Lehman and Woodward, 2008), they must be accurately reconstructed. The process of estimating the number of LAGs eroded since birth is termed retrocalculation and involves one of several methods, including (1) visual alignment of an ontogenetic series of LAG sequences (e.g., Chinsamy, 1993; Castanet, 1994; Erickson and Tumanova, 2000; Bybee et al., 2006); (2) measurement of the thickness of bony tissue between successive LAGs (e.g., Horner and Padian, 2004; Klein and Sander, 2007; Xu et al., 2007; Hübner, 2012); or (3) regression analysis to fit a set of growth models to a LAG sequence and information theory to select the best model for retrocalculation (Cooper et al., 2008; Tsuihiji et al., 2011; Lee et al., 2013). Although the first two methods are computationally simple, the former tends to minimize variation in growth (thus biasing variation studies), whereas the latter requires subjectivity in selecting a particular thickness measurement for retrocalculation. The third method is more computationally involved but provides an assessment of how well the data actually support the resulting age estimates. More importantly, this method takes into account that sequentially sampled growth data are not independent, which is a required assumption in regression analysis to allow accurate assessment of confidence intervals (Cooper et al., 2008; Lee et al., 2013).

Process-Error Models—Two factors preclude simpler methods of retrocalculation. First, each LAG sequence reflects repeated measurements of an individual during the course of ontogeny such that the resulting data points are not independent. Second, potential loss of the early growth record to bone remodeling means that the preserved LAG sequences may not be calibrated to absolute time (i.e., simple counts of LAGs underestimate age). Therefore, this longitudinally sampled (not to be confused with longitudinal cuts) growth data cannot be fitted to traditional observation-error growth models (e.g., Richards, 1959; Gaillard et al., 1997) but instead must be fitted to process-error models (Cooper et al., 2008; Lee et al., 2013). Failure to incorporate process-error models in a longitudinally sampled data set leads

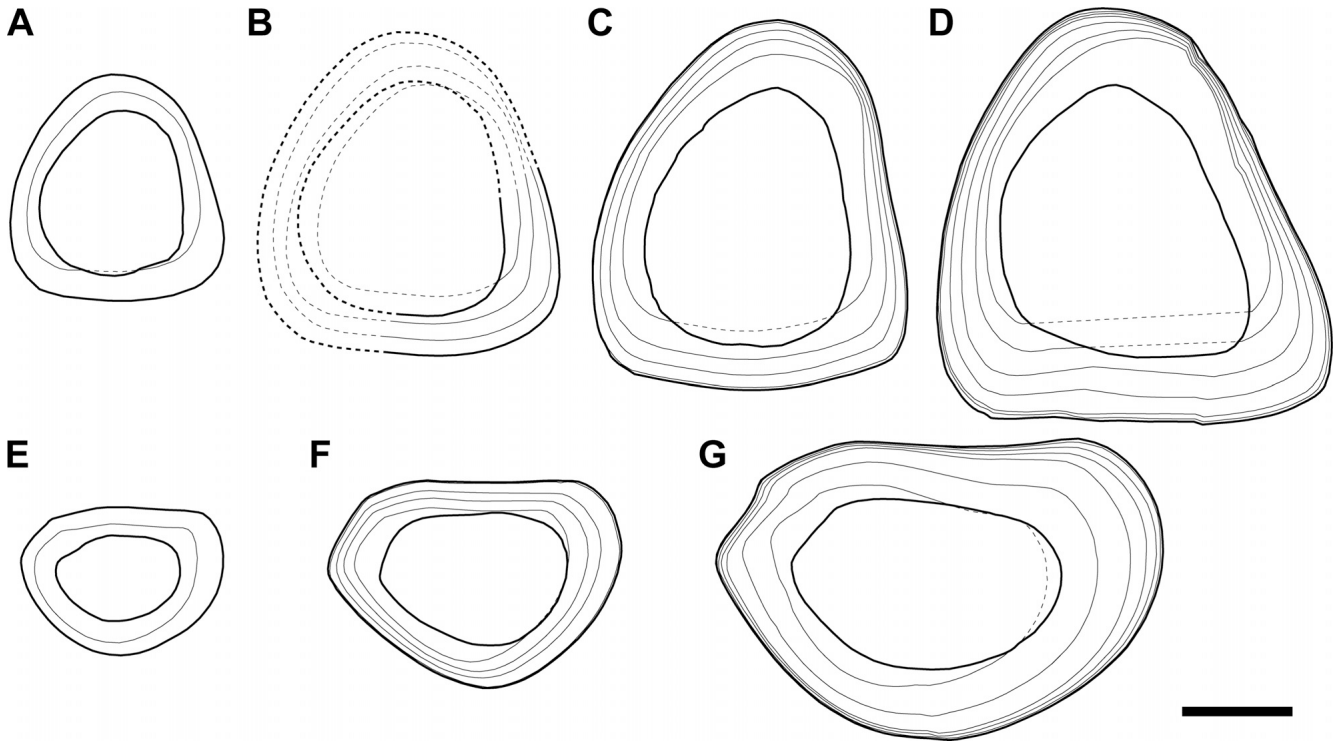

FIGURE 2. Mid-diaphyseal transverse sections of sampled femora (**A**–**D**) and tibiae (**E**–**G**). **A**, FMNH PR 2153; **B**, FMNH PR 2150; **C**, FMNH PR 2215; **D**, FMNH PR 2123; **E**, FMNH PR 2152; **F**, UA 8710; **G**, UA 8685. Thick lines represent periosteal and endosteal borders, whereas thin lines represent annual growth lines. Dashed lines are reconstructions. For all sections, cranial points upward and lateral points to the left. Scale bar equals 5 mm.

to overly narrow confidence intervals and an increased risk in the false rejection of a null hypothesis (Brisbin et al., 1987). These models assume that observations are relatively free of measurement error and that each prediction at time t + 1 is a function of the observation from the current time period t. Unfortunately, the structure of the models precludes the analysis of LAG sequences containing fewer than two LAGs. Thus, FMNH PR 2153 and FMNH PR 2152, both of which contain a single LAG, were excluded from the model-based regression analysis.

Because no single model describes all vertebrate growth patterns (e.g., Zullinger et al., 1984), we evaluated seven alternative process-error models. These are described generally by the following two difference equations:

$$C_{t+1} = C_t + G, \tag{1}$$

$$C_{t+1} = \mathrm{A}\left[1 + \exp(-K)\left[\left(\frac{C_t}{A}\right)^{1-m} - 1\right]\right]^{\frac{1}{1-m}}, \tag{2}$$

where C_t is the LAG circumference at time t, C_{t+1} is the LAG circumference at time t + 1, G is the absolute growth rate, A is the asymptotic circumference, K is the mean relative growth rate, and m is the shape parameter. Note that absolute time is effectively factored out of both equations, so the a priori knowledge of the ontogenetic age of a given specimen is unnecessary. Equation 1 is simply the linear model (growth at a constant rate lasting an unlimited length of time) as expressed in the form of a difference equation. Although we recognize that vertebrates rarely grow linearly (i.e., at a constant rate) throughout the entire span of ontogeny, we include the linear model in set of candidate models to test whether the collected growth data are robust enough to support complex and biologically realistic sigmoidal models. Equation 2 is a reparameterized form of the Richards sigmoidal (asymptotic-growth) model (Richards, 1959). By substituting fixed values of m, we converted the Richards model into specific sigmoidal models that differ primarily in inflection point (i.e., where size is still increasing substantially but the rate of growth is just beginning to decelerate). Thus, it occurs prior to birth in the monomolecular model (m = 0); at 0.30A in the von Bertalanffy model (m = 2/3); at 0.37A in the Gompertz model (m ≈ 1); at 0.50A in the logistic model (m = 2); at 0.63A in the extreme value function model (m = 4); and at 0.75A in an innominate model (m = 8.4).

Age Estimation Using Regression and Double Optimization

Cooper et al. (2008) used fixed-effects regression to estimate the parameter values for each model, which was appropriate given that only a single individual was analyzed. Fixed-effects regression, however, is not appropriate for our femoral and tibial data sets, each of which represents several individuals. To account for intraspecific variation, we modeled growth curve parameters as the sum of a fixed (mean) component common to all specimens and a random (idiosyncratic) component specific to each specimen. This method of mixed-effects regression assumes that a single mean growth pattern exists (e.g., Gompertz) and individual growth profiles vary about that mean (e.g., variation in asymptotic size or relative growth rate) (Aggrey, 2009). Moreover, mixed-effects regression is appropriate when the number of observations in specimens is unequal (Lindstrom and Bates, 1988; Vonesh and Carter, 1992), as is the case here with the variable number of LAGs per specimen.

We fitted each of the seven candidate growth models to the respective femoral and tibial data and estimated fixed and random effects. For each specimen, seven alternative estimates of age were calculated using the following reversed integrated-time versions of Equations 1 and 2:

$$t_C = -\frac{1}{G}C - \frac{A_0}{G} - t_{\mathrm{missing}}, \tag{3}$$

$$t_C = -\frac{1}{K}\ln\left[-\frac{C^{1-m} - A^{1-m}}{A^{1-m} - A_0^{1-m}}\right] - t_{\mathrm{missing}}, \tag{4}$$

where t_C is the number of years (LAGs) preserved in the bone with a circumference C, G is the growth rate, A is the asymptotic circumference, K is the mean relative growth rate, m is the shape parameter, A_0 is the bone circumference at birth, and $t_{missing}$ is the retrocalculated time missing from the growth record of each specimen.

To date, neither neonatal specimens nor eggs have been attributed to *Masiakasaurus*. In order to estimate an upper limit of egg and thus neonatal size, we reflected an image of a cranial view of a left pubis (Carrano et al., 2002:fig. 13) about the vertical axis and measured the horizontal distance between the proximal end of the left pubis and its reflection. The resulting estimate of minimum pelvic canal diameter suggests that an egg of *Masiakasaurus* was probably no larger than that of *Alligator mississippiensis*. If both neonates were similar in size, based on measurements of *Alligator* (Lee, 2004), we expect the femoral and tibial mid-diaphyseal circumferences of *Masiakasaurus* to be approximately 6.3 mm at hatching. Optimal values of neonatal bone circumference (A_0) and retrocalculated time ($t_{missing}$) for each specimen were calculated simultaneously by minimizing the residual sum of squares (i.e., double optimization). To allow for individual variation in hatching size, we constrained the possible values of A_0 to range between 0 and 13 mm. In addition, $t_{missing}$ was constrained to integer values because the minimum temporal resolution between sequential LAGs is 1 year (e.g., Morris, 1970; Frylestam and Schantz, 1977; Hemelaar and Van Gelder, 1980; Hutton, 1986; Castanet, 1994; Castanet et al., 2004; de Ricqlès et al., 2004; Köhler et al., 2012). The age of each specimen was estimated by summing the optimized value of $t_{missing}$ and t_c. Table 1 lists the estimated ages of specimens using different models of retrocalculation.

Selection of the Best Model for Age and Life-History Estimation

The set of alternative models and age estimates was discriminated using the small-sample corrected form of Akaike's information criterion (AIC_c) (Hurvich and Tsai, 1989). In contrast to other information criteria (e.g., AIC or BIC), AIC_c tends to select the 'true' model more frequently when the sample size is small (Azari et al., 2006), making it appropriate for the current study. AIC_c values are often similar to one another (especially in models that share a similar form), so strength of support was calculated by taking the difference in AIC_c (ΔAIC_c) values between each alternative model and the best model (Table 2). Thus, the model with the strongest support (i.e., the best model) has a ΔAIC_c value equal to 0, whereas a poorly supported model has a ΔAIC_c value of ≥2 (Burnham and Anderson, 2002). Although we generally selected the model with the lowest ΔAIC_c value, an alternative model with a ΔAIC_c value <2 was considered if it predicted a reasonable neonatal bone circumference (Table 3) and if it correctly predicted the number of LAGs preserved in specimens that could not be analyzed using regression (only specimens with at least two LAGs can be analyzed by mixed-effects regression).

Estimates of growth and life-history traits were calculated from the best femoral and tibial growth models (Table 4). Asymptotic bone circumference, maximum growth rate ($AKm^{(m/(1-m))}$), age at inflection (I), and growth duration (i.e., time needed to grow

TABLE 2. Mean parameters and ΔAIC_c values of growth models.

Element	Model	A (mm)	K (year^{-1})	A_0 (mm)	I (year)	AIC_c	ΔAIC_c
Femur	Monomolecular	70.3	0.20	12.6	−1.0	40.74	0.0
	von Bertalanffy	63.0	0.33	9.4	1.1	41.41	0.7
	Gompertz	62.2	0.36	9.6	1.7	41.35	0.6
	Logistic	60.2	0.47	8.4	3.8	41.50	0.8
	Extreme value function	57.3	0.72	7.9	7.1	42.69	2.0
	Innominate	54.8	1.25	7.1	10.5	45.37	4.6
	Linear	N/a	4.2	8.2	N/a	46.10	5.4
Tibia	Monomolecular	57.3	0.42	10.4	−0.5	37.98	3.6
	von Bertalanffy	57.1	0.42	10.6	0.6	36.28	1.9
	Gompertz	57.0	0.45	7.6	1.6	35.58	1.2
	Logistic	56.7	0.54	8.1	3.3	34.40	0.0
	Extreme value function	56.3	0.74	8.5	6.2	35.97	1.6
	Innominate	56.4	1.26	6.5	11.0	42.41	8.0
	Linear	N/a	3.32	7.4	N/a	51.52	17.1

Abbreviations: **A**, asymptotic bone circumference; **K**, relative or absolute growth rate; $\mathbf{A_0}$, neonatal bone circumference; **I**, age at inflection.

to 95% full size) were either extracted directly from parameter estimates or calculated from the following equations:

$$I = -\frac{1}{K}\ln\left[-\frac{(m-1)A^{1-m}}{A^{1-m}-A_0^{1-m}}\right], \quad (5)$$

$$t_{95A} = I - \frac{1}{K}\ln\left[\frac{0.95^{1-m}-1}{m-1}\right], \quad (6)$$

Uncertainty associated with parameter estimates was propagated into calculations of life-history traits using parametric bootstrapping (Dennis and Taper, 1994) to generate 95% confidence intervals. All analyses were performed in R version 2.13.0 (R Development Team, 2011).

RESULTS

Bone Histology of *Masiakasaurus*

General Patterns—Femoral and tibial bone histology of *Masiakasaurus* share some features typical to other non-avian theropods (e.g., Chinsamy, 1990; Varricchio, 1993; de Ricqlès et al., 2003; Horner and Padian, 2004; Padian et al., 2004; Bybee et al., 2006; Erickson et al., 2009; D'Emic et al., 2012). Both elements have compact cortices that are distinctly zonal. Wide zones of parallel-fibered or fibrolamellar matrix contain numerous vascular canals showing localized longitudinal, reticular, and plexiform organization (Fig. 3). In contrast, adjacent zones are separated by a thin and poorly vascularized annulus. The annulus consists predominately of parallel-fibered bone matrix and is bordered externally by a single LAG, although a doublet LAG is also common (Fig. 3). In the largest tibial specimen, zones and annuli are compressed subperiosteally to form an external fundamental system (EFS), effectively marking the completion of bone growth (Fig. 3).

Femora and tibiae all have an open medullary cavity, and the normal expansion of this cavity is visible when the sections are ordered in ascending size (Fig. 2). In the smaller specimens, the endosteal margin is scalloped and clearly crosses the 'grain' of the cortex, both of which suggests peripherally directed, endosteally mediated resorption. Larger specimens, however, show an endosteal margin that is internally lined by lamellae, suggesting the completion of medullary cavity expansion. The tempo of medullary cavity expansion is slower than the rate of periosteal growth such that femoral and tibial cortices thicken with size and age (Fig. 2).

Osteonal remodeling is not random, but rather is positively correlated with size and age. Secondary osteons first appear along the innermost cortex, with a remodeling front that shifts with increasing size towards the periosteal surface. Moreover, the distribution of osteonal remodeling across a section is highly localized but varies between limb elements, similar to that reported in *Allosaurus* and *Acrocanthosaurus* (Bybee et al., 2006; D'Emic et al., 2012). Using elliptically polarized light, all specimens show an optical behavior of negative elongation, which suggests replacement of collagen with secondary apatite.

Femur—Specimens span three size classes: small (midshaft circumference <40 mm), intermediate (midshaft circumference ≈45 mm), and large (midshaft circumference >50 mm). The smallest specimen (FMNH PR 2153; midshaft circumference = 33.6 mm, estimated bone length approximately 130 mm) shows several histological features associated with juvenile bone. Cortical vascularization is intense, with predominately reticular to plexiform canals. Only a single LAG with a thin annulus is present, with a partially eroded caudomedial border. No circumferential lamellae occur along the endosteal margin, which is clearly resorptive. A few secondary osteons are present but these are restricted to an area of $600 \times 600\ \mu m^2$ along the craniomedial endosteal margin. This area also features a small amount of compacted coarse cancellous bone, and its presence at midshaft reflects the incorporation of a portion of the metaphysis from an

TABLE 3. Neonatal bone circumference (mm) estimated using regression coefficients and double optimization.

Element	Specimen	Model 1	Model 2	Model 3	Model 4	Model 5	Model 6	Model 7
Femur	FMNH PR 2150	12.6	12.6	8.3	8.0	6.6	7.7	9.6
	FMNH PR 2215	12.6	7.4	9.6	8.8	7.7	6.9	7.8
	FMNH PR 2123	12.6	8.1	10.8	8.3	7.1	6.8	7.3
Tibia	UA 8710	8.2	8.5	7.4	7.5	6.7	6.8	7.1
	UA 8685	12.6	12.6	7.8	8.7	6.5	6.3	7.6

Abbreviations: **1**, monomolecular; **2**, von Bertalanffy; **3**, Gompertz; **4**, logistic; **5**, extreme value function; **6**, innominate; **7**, linear.

TABLE 4. Individual and mean parameters of the logistic growth curves.

Element	Specimen	A (mm)	K (year^{-1})	I (year)	A_0 (mm)	GD (year)
Femur	FMNH PR 2150	57.3	0.51	3.5	8.0	9.2
	FMNH PR 2215	56.9	0.52	3.3	8.8	8.9
	FMNH PR 2123	66.2	0.39	4.9	8.3	12.5
	Mean	60.0 (55.4, 68.3)	0.47 (0.34, 0.63)	3.8 (2.7, 6.1)	8.4 (6.7, 9.2)	10.0 (7.4, 14.7)
Tibia	UA 8710	56.7	0.22	8.3	7.5	21.4
	UA 8685	56.7	0.86	1.9	9.7	5.4
	Mean	56.7 (51.4, 59.7)	0.54 (0.20, 0.89)	3.3 (1.7, 10.2)	8.1 (6.5, 10.3)	8.8 (5.1, 24.4)

Parentheses enclose the 95% confidence intervals of the mean parameters. **Abbreviations**: **A**, asymptotic bone circumference; **K**, relative growth rate; **I**, age at inflection; **A_0**, neonatal bone circumference; **GD**, growth duration.

earlier point in ontogeny into the diaphysis at the present stage of ontogeny as the bone grows in length (metaphyseal reduction sensu Enlow, 1963). This differs somewhat from osseous or cortical drift in which diaphyseal bone is resorbed and redeposited to laterally shift the longitudinal axis during the development of bone curvature (Enlow, 1963). In contrast to juvenile bone from other non-avian theropods, the cortical bone matrix in this specimen is not predominately woven-fibered. Instead, it is parallel-fibered as demonstrated by relatively lenticular osteocytic lacunae and bulk bright birefringence (transversely oriented crystallites) under circular polarization (Fig. 4A, B).

The intermediate specimen (FMNH PR 2150; midshaft circumference = 48.4 mm, estimated bone length approximately 160 mm) was taken from the proximal half of a fragmentary femur. At the standardized level of sectioning, only the caudomedial cortex is preserved, and consequently, the section is incomplete. Nevertheless, we included this specimen in our analysis because it is the only available representative of the intermediate size class. FMNH PR 2150 has zonal cortical bone in which thick zones of parallel-fibered matrix are perforated by longitudinal to circumferential canals and alternate with thin parallel-fibered annuli (Fig. 4C). Each annulus contains a set of LAGs, totaling three sets in the cortex. The innermost set of LAGs is a doublet and is partially eroded by the endosteal margin. Taken together with the lack of endosteal lamellae, the medullary cavity was still expanding before death.

Two specimens were sectioned from the large size class. The smaller of the two specimens (FMNH PR 2215; midshaft circumference = 53.0 mm, bone length = 180.0 mm) has an inner cortex composed of similar parallel-fibered zones and annuli as found in the previous size classes (Fig. 4D, E). However, a subtle histological change occurs in all but the caudal cortex beyond the third preserved LAG (approximately 87% femoral circumference), where the zones appear thin and poorly vascularized, particularly those closest to the periosteal margin. However, an external fundamental system is not clearly developed. Nevertheless, the histology is consistent with reduced growth leading up to the time of death. Four sets of LAGs are preserved in the cortex. Although the innermost LAG is partially eroded by the caudal expansion of the medullary cavity, lamellae line the entire endosteal margin, suggesting that the expansion of the medullary cavity was complete prior to death.

The largest specimen (FMNH PR 2123; midshaft circumference = 62.9 mm, bone length = 202.5 mm) is similar in many regards to FMNH PR 2215, but does exhibit the following differences. First, FMNH PR 2123 contains a small amount of fibrolamellar bone that appears restricted to the caudomedial cortex (Fig. 4F), with parallel-fibered matrix dominating the remainder of the cortex. Second, the change to poorly vascularized matrix in the outer cortex occurs at 97% femoral circumference at a size relatively larger than in FMNH PR 2215. Third, FMNH PR 2123 preserves two more LAGs than FMNH PR 2215 does for a total of six LAGs. Finally, endosteal deposits are approximately two times thicker in FMNH PR 2123 than in FMNH PR 2215, indicating that the expansion of the medullary cavity stopped long before death.

Tibia—Specimens span three size classes: small (midshaft circumference <30 mm), intermediate (midshaft circumference ≈40 mm), and large (midshaft circumference >50 mm). The smallest specimen (FMNH PR 2152; midshaft circumference = 26.2 mm, estimated bone length approximately 110 mm) has cortical bone that is stratified into inner and outer parallel-fibered zones separated by a parallel-fibered annulus and a LAG (Fig. 5A, B). The zones are packed with vascular canals, which tend to be longitudinally oriented on the caudal side but reticular to plexiform elsewhere. In contrast, the relatively sparse vascularization in the annulus takes the form of longitudinal canals. Numerous Sharpey's fibers radially perforate the annulus in the craniolateral cortex. Despite the high density of Sharpey's fibers in this region, osteonal remodeling is not apparent here or elsewhere in the cortex. Endosteal lamellae were deposited before death, but resorption effaced them, leaving only islands of lamellae on the craniolateral and caudal endosteal margins.

The intermediate-sized tibia (UA 8710; midshaft circumference = 37.1 mm, estimated bone length approximately 140 mm) is generally similar to FMNH PR 2152 but differs in the following ways. Three additional LAGs are present for a total of four. Although the innermost zone is partially eroded by the medullary cavity, it is still more than twice the thickness of the three successively external zones. This sharp transition in zone thickness occurs at the first preserved LAG (approximately 73% tibial circumference). There is no apparent change in the quality of the bone matrix as zones on either side of the transition exhibit moderate bulk birefringence, consistent with parallel-fibered matrix being composed of obliquely to transversely oriented crystallites (Fig. 5C, D). Orientation and density of cortical vascularization are similar across the transition, although there is a slight reduction in density that is restricted to the caudal cortex. Unlike that of the small tibia, the mottling in the craniolateral cortex is accompanied by at least two generations of secondary osteons. They do not extend all the way to the periosteal margin and are restricted to the inner half of the cortex. Endosteal lamellae are only preserved along the lateral, cranial, and craniomedial margins of the medullary cavity, suggesting that expansion of the cavity was slowing just prior to death.

UA 8685 (midshaft circumference = 57.1 mm, bone length = 205.4 mm) is the largest of the sampled tibiae and not unexpectedly records the longest growth record. It preserves seven sets of mostly doublet LAGs, two of which comprise the external fundamental system (EFS) (Fig. 3). The inner three zones are noticeably thicker than those of the smaller specimens. In addition, they contain a complex mixture of parallel- and woven-fibered matrices with reticular to plexiform vascularization (Fig. 5E, F). The thickness of these zones is noticeably greater in this specimen than in the smaller ones (Fig. 2E–G). Beyond the third preserved LAG (approximately 91% of tibial circumference), the

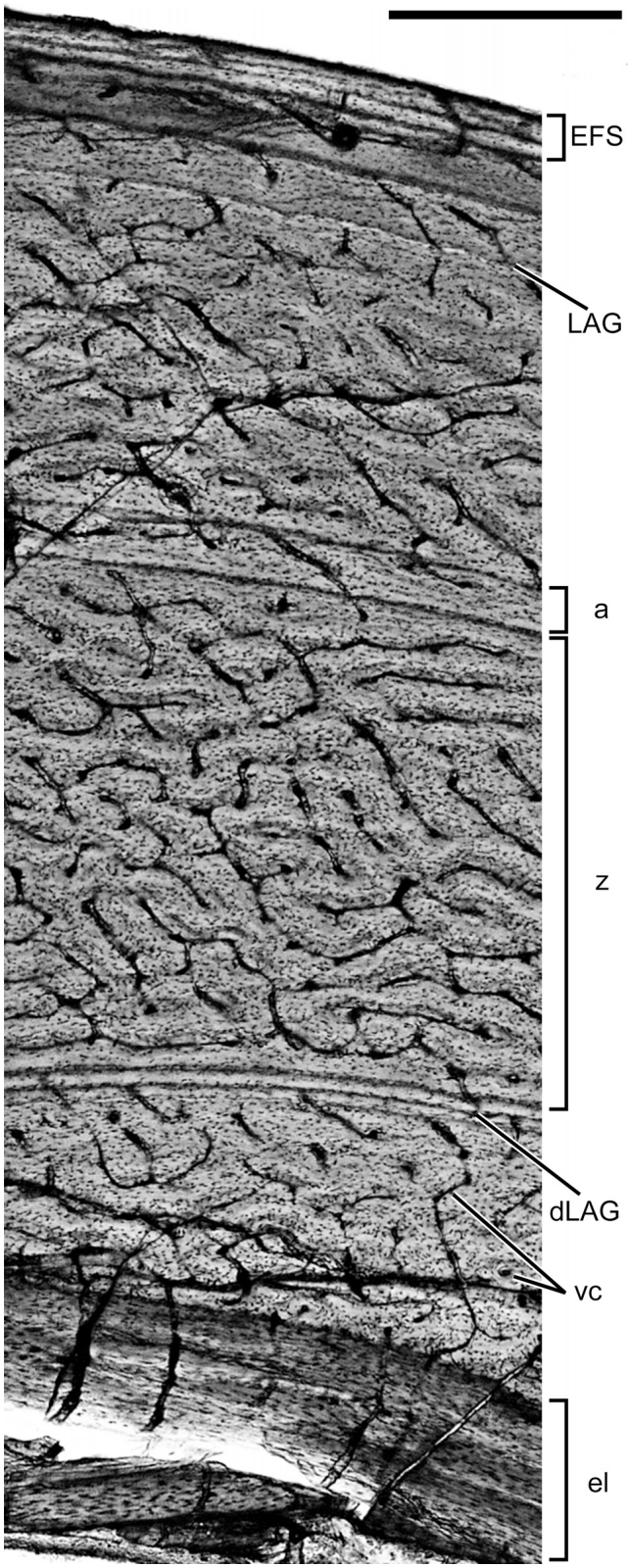

FIGURE 3. Bone microstructure in the tibia of *Masiakasaurus knopfleri* (UA 8685) showing general histological patterns. **Abbreviations**: **a**, annulus; **dLAG**, doublet growth line; **EFS**, external fundamental system; **el**, endosteal lamellae; **LAG**, line of arrested growth (growth line); **vc**, vascular canal; **z**, zone. Scale bar equals 500 μm.

remaining outer zones thin substantially and have few vascular canals. The parallel-fibered matrix in these zones show a strong birefringence, suggesting that transversely oriented crystallites are generally more prominent in the outer cortex than in the inner one. Osteonal remodeling is extensive and spans almost the entire thickness of the cortex albeit still localized to the craniolateral side. Thick deposits (up to 500 μm) of endosteal lamellae completely line the medullary cavity (Fig. 3), indicating that the medullary cavity completed its expansion long before death.

Age Estimation and Growth Curve Reconstruction

Selection of the 'Best' Growth Model—Age estimates for femoral and tibial specimens ranged from 1 to 20 and 1 to 17 years, respectively, depending on the model that was used for retrocalculation (Table 1). The linear model is least supported in both the femoral and tibial data sets (Table 2), so we rejected the plausibility of the old age estimates predicted by this model. For similar reasons, we rejected the femoral age estimates based on the extreme value function and innominate models as well as tibial age estimates based on the monomolecular and innominate models. Of the remaining four plausible models describing femoral growth, we did not further consider the monomolecular, von Bertalanffy, and Gompertz models because they predict unreasonably large neonatal size in some of the specimens (Table 3). Thus, we selected the logistic model to describe femoral growth because it fits the data well and predicts reasonably sized neonates. Similarly for the tibial data, the von Bertalanffy model overpredicts neonatal size, leaving three plausible models. Among them, we selected the logistic model to represent tibial growth because it has the lowest ΔAIC_c value (0).

Mean Growth Patterns of the Femur and Tibia—The mean growth curves of the femur and tibia have broadly similar appearances and properties (Fig. 6; Table 4). Mean asymptotic midshaft circumference is only 6% larger in the femur (60.0 mm) than in the tibia (56.7 mm). On average, femora and tibiae experienced maximum rates of circumferential growth (i.e., the inflection point) when they were 3.8 and 3.3 years old, respectively. At these ages, femoral circumference grew 7.1 mm/year, whereas tibial circumference grew slightly faster at 7.4 mm/year. Even when size differences are accounted for by comparing the size-standardized mean relative growth rate (K/m), circumferential growth is slower (13%) in the femur than in the tibia. Growth was effectively complete (at 95% asymptotic size) about 1 year later in the femur (10.0 years) than in the tibia (8.8 years).

Individual Variation in Growth—Even with the low sample size examined herein, we found moderate to substantial individual variation in growth (Fig. 6B, D). Among the sampled femora, FMNH PR 2123 is estimated to have the largest size asymptote, but grew at the slowest rate and for the longest duration (Table 4). Even more striking individual variation is estimated in the tibial sample. Mixed-effects modeling predicts that both UA 8710 and UA 8685 have identical asymptotic sizes but differ in projected growth duration, which is four times shorter in UA 8685 than in UA 8710 (Table 4).

We could not directly estimate how differently FMNH PR 2153 and FMNH PR 2152 grew relative to the other femora and tibiae because each specimen only contains a single LAG (Table 1). Consequently, they were not included in the regression analysis, which requires that LAG sequences contain at least two LAGs. Instead, we used the corresponding mean growth trajectory to calculate the ontogenetic age of these specimens, which are estimated to be 3 years old at death. Moreover, the mean growth trajectories correctly predict that both specimens should only preserve one cortical LAG each given their respective endosteal circumferences (23.4 and 15.6 mm). Therefore, growth rate and

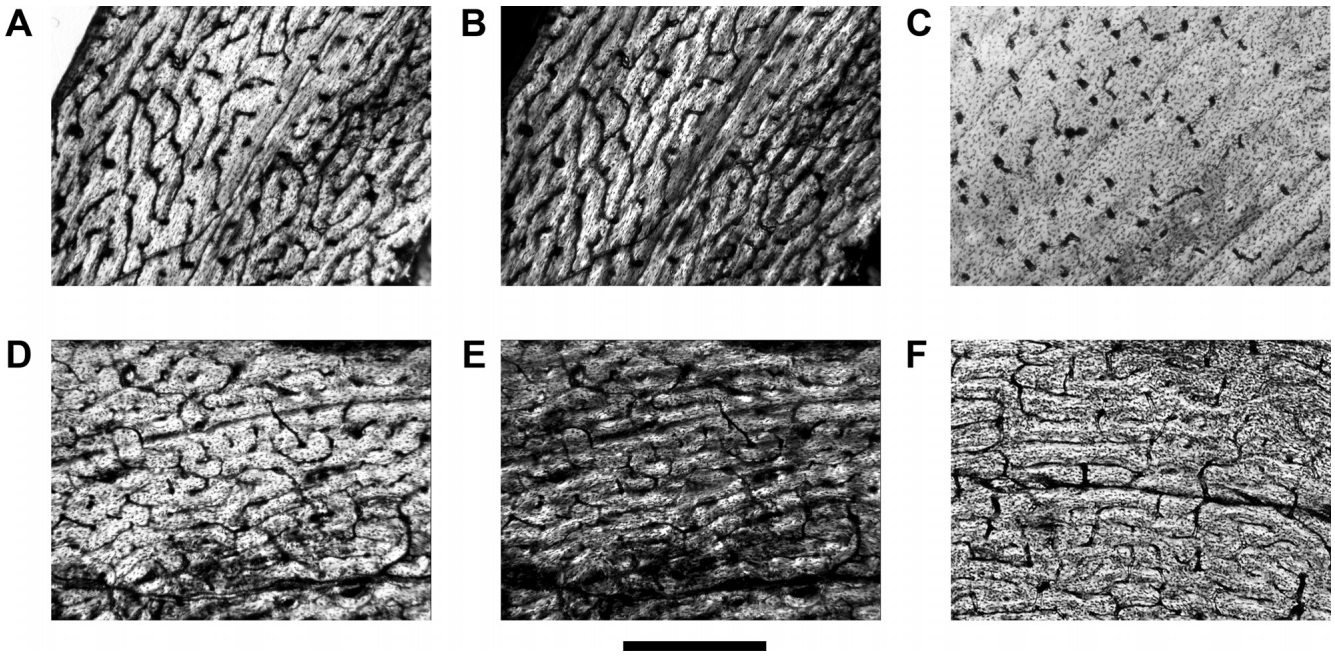

FIGURE 4. Microstructural organization of femora in a growth series of *Masiakasaurus knopfleri*. **A**, FMNH PR 2153, non-polarized; **B**, same specimen under circularly polarized light (CPL); **C**, FMNH PR 2150, non-polarized; **D**, FMNH PR 2215, non-polarized; **E**, same specimen under CPL; **F**, FMNH PR 2123, non-polarized. CPL images have a 0.8 gamma correction to accurately reproduce the polarization luminance in print. Bright regions indicate transversely oriented crystallites, whereas dark regions indicate longitudinally oriented crystallites. Black regions are non-bone. Scale bar equals 500 μm.

duration in FMNH PR 2153 and FMNH PR 2152 likely approximated the populational mean (Fig. 6A, C).

DISCUSSION

Determinate Growth

As with most terrestrial and aquatic vertebrates (Sebens, 1987), *Masiakasaurus* exhibits determinate growth. Histological evidence of this was found in the largest sampled tibia (UA 8685), which preserves an external fundamental system (EFS). The EFS has characteristics of extremely slow-growing bony tissue (e.g., avascularity and tightly spaced growth lines) and is widely accepted as a histological proxy for the completion of skeletal growth (e.g., Cormack, 1987; Chinsamy, 1990; Horner et al., 1999; de Ricqlès et al., 2003; Erickson et al., 2004; Sander et al., 2006; Xu et al., 2006; Köhler and Moyà-Solà, 2009; Woodward et al., 2011). Because the EFS also contains two LAGs, the individual represented by UA 8685 lived for at least 2 years after reaching full body size (Fig. 3). Given that UA 8685 is the largest known tibia of *Masiakasaurus*, our findings confirm that individuals were skeletally mature at a small body size. They also provide taxonomic insight into the identity of fragmentary noasaurid taxa of the coeval Lameta Formation in India. Because the Lameta noasaurids are larger but otherwise morphologically similar to *Masiakasaurus*, the differences in size might reflect ontogenetic effects (Carrano et al., 2011). Evidence of skeletal maturity in *Masiakasaurus*, however, strongly suggests that the Lameta taxa are indeed distinct larger-bodied forms.

Growth Trajectory

When viewed with polarized light, the femoral and tibial cortices of *Masiakasaurus* exhibit a bulk optical luminosity that is characteristic of parallel-fibered bone (Figs. 4, 5). In extant amniotes, parallel-fibered bone tends to grow slowly. Although measurements using fluorescent bone labels reveal rates as fast as 30 μm per day, slower growth rates between 3 and 10 μm per day are more typical (Roberts et al., 1988; de Margerie et al., 2002; Castanet et al., 2004). Given this range of actualistic growth rates and the prevalence of parallel-fibered bone in our histological sample, *Masiakasaurus* likely grew slowly throughout ontogeny.

Measurements of LAG circumference and growth curve reconstruction reveal that the average individual took about 8–10 years to get to the equivalent skeletal size of a Great Dane (Fig. 6A, C; Table 4). Skeletal growth rates peaked early, around 3–4 years of age, yet even during this period femoral and tibial midshaft circumferences only increased about 7 mm per year. When converted to a rate of radial deposition and adjusted for an annual growing period of 371 Maastrichtian days (Lee et al., 2013:equation 1), this peak rate amounts to 3 μm per day. If instead we assume that the annual growing period was a half-year comparable to extant crocodylians (Lance, 2003), the depositional rate doubles to 6 μm per day. Either estimate supports our qualitative assessment of growth based solely on histological texture and suggests a relatively slow growth in *Masiakasaurus*.

Slow-growing dinosaurs draw inevitable comparisons to crocodylians. We reanalyzed seven femoral sections from female Louisiana alligators that were prepared for an earlier study (Lee, 2004) and added an additional specimen for better ontogenetic coverage (Supplementary Data, Table S1). Using mixed-effects modeling, we found that the extreme value function best fits the data (alternative models have ΔAIC_c values from 3.9 to 28.4; Supplementary Data, Table S2). This model predicts the mean age at inflection at 9 years with a 95% confidence interval between 7 and 14 years (Supplementary Data, Table S3), which brackets when female alligators living in the estuarine wetlands of Louisiana become sexually mature (~8 years according to Rootes et al., 1991). Having demonstrated the accuracy of the growth model, we calculated the mean relative growth rate

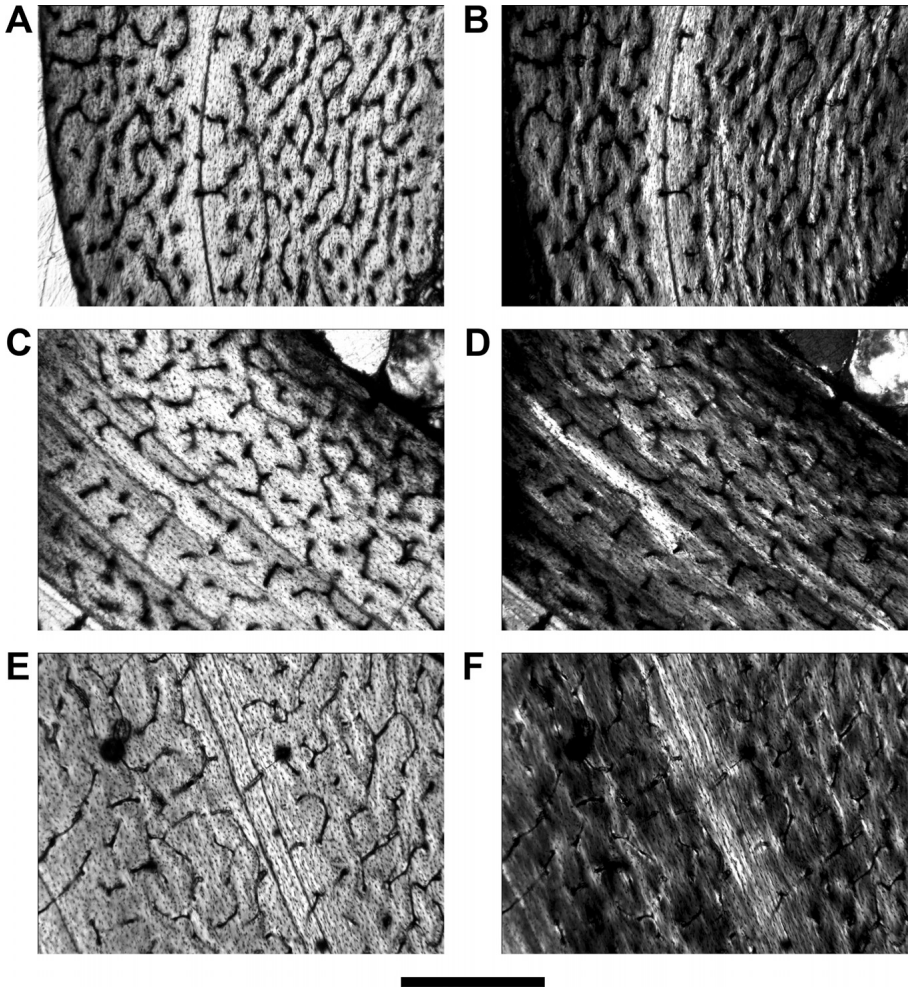

FIGURE 5. Microstructural organization of tibiae in a growth series of *Masiakasaurus knopfleri*. **A**, FMNH PR 2152, non-polarized; **B**, same specimen under circularly polarized light (CPL); **C**, UA 8710, non-polarized; **D**, same specimen under CPL; **E**, UA 8685, non-polarized; **F**, same specimen under CPL. CPL images have a 0.8 gamma correction to accurately reproduce the polarization luminance in print. Bright regions indicate transversely oriented crystallites, whereas dark regions indicate longitudinally oriented crystallites. Black regions are non-bone. Scale bar equals 500 μm.

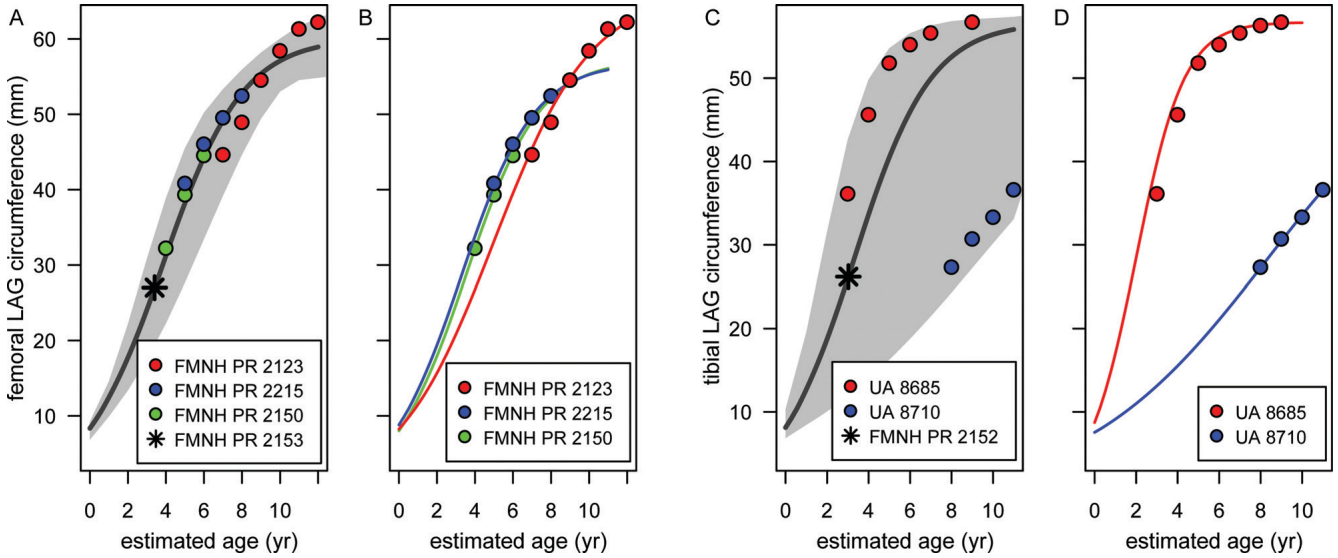

FIGURE 6. Growth profile of *Masiakasaurus knopfleri*. **A**, mean femoral trajectory; **B**, individual femoral trajectories; **C**, mean tibial trajectory; **D**, individual tibial trajectories. LAG circumference is used as proxy for size because each LAG represents the bone perimeter at the end of an annual growth period. Specimens that could not be included in the mixed-effects analysis because they contained less than two LAGs are marked by an asterisk. Gray bands indicate 95% confidence intervals.

(K/m = 0.143) and the growth duration (14 years). The results suggest that the alligator grew 40% slower and took 40% more time to reach skeletal maturity than *Masiakasaurus* did. Therefore, despite slow rates, the maximum growth (and presumably metabolic rate) of *Masiakasaurus* still outpaced that of a representative extant crocodylian.

Our assessment of growth in *Masiakasaurus* is strikingly different than in comparably sized non-avian theropods. The coelophysoid *Coelophysis*, basal ceratosaur *Limusaurus*, and paravians *Conchoraptor*, *Byronosaurus*, and *Velociraptor* all have long bone cortices composed predominately of fibrolamellar bone (Chinsamy, 1990; Padian et al., 2004; Erickson et al., 2009; Xu et al., 2009), which generally forms faster than parallel-fibered bone (de Margerie et al., 2002). In addition, preliminary growth analyses of *Coelophysis* and *Limusaurus* suggest that the largest sampled individuals were 4–6 years old at death (Chinsamy, 1990; Erickson et al., 2001). Although precise data are not yet available for *Conchoraptor*, *Byronosaurus*, and *Velocirator*, we expect broad similarity to *Coelophysis* and *Limusaurus* given the histological similarities among them. If correct, growth was about 40% slower in *Masiakasaurus* than in these non-avian theropods, suggesting a strong deviation from the general scaling continuum across non-avian theropods.

Reasons for this deviation are not yet clear and may involve phylogenetic or ecological factors. In well-sampled clades such as the Tyrannosauridae, variation in growth rates can be viewed in the context of heterochrony (Erickson et al., 2004). However, virtually nothing is known about the growth of ceratosaurs, which might have as a group evolved slower growth rates. We would expect then that maturity at small size in *Masiakasaurus* reflects an early offset of growth or progenesis. If instead growth rates in basal ceratosaurs followed the general scaling continuum for non-avian theropods, the slow growth of *Masiakasaurus* reflects neoteny and progenesis. In either heterochronic scenario, slowed growth could be ecologically advantageous. Paleoecological reconstructions of the Maevarano Formation based on sedimentological and faunal data suggest a highly seasonal, semiarid climate that stressed at least seasonally the terrestrial fauna (Rogers et al., 2007). Given that experimental studies have demonstrated the evolution of slow growth in response to environments with chronically low resources (Arendt and Reznick, 2005), it is plausible that *Masiakasaurus* evolved reduced growth rates to minimize structural and maintenance costs.

Growth Variation and Dimorphism

Mixed-effects modeling suggests that individuals of *Masiakasaurus* did not necessarily mature at the same size or age (Fig. 6B, D; Table 4). The variation in growth trajectories may reflect developmental plasticity, which has been inferred for other dinosaurs (e.g., Sander and Klein, 2005). Although the ability to accommodate to changing environmental conditions during growth can be advantageous, we do not find evidence that developmental plasticity acted throughout ontogeny. The full-grown specimen UA 8685 shows no substantial bone deposition beyond the EFS. Moreover, instead of randomly spaced LAGs and jagged growth trajectories, our examinations reveal gradual attenuation. We interpret these results as developmental plasticity that is restricted to early ontogeny. During this sensitive period of development, the characteristics of an individual (e.g., growth rate and maximum size) are set through a complex interaction of genetic and epigenetic (environmental) factors. Beyond this period, the developmental pathway canalizes, and environmental influences may have little or no effect (Bateson et al., 2004).

Masiakasaurus not only shows variation in growth but also in skeletal form. Carrano et al. (2002) reported that the presence of prominent muscle scars on the femur and tibia as well as fusion between tibia and astragalocalcaneum tend to occur in 'robust' specimens, thereby providing some basis for recognizing 'robust' and 'gracile' morphs. When we parsed the growth profiles of individual specimens by morph (Table 1), we found no clear trend in asymptotic size or growth rate for either morph. The only 'robust' specimens in our sample (FMNH PR 2123 and UA 8685) do not necessarily have largest asymptotic size or the fastest growth rate (Table 4). Interestingly, these specimens are at 95–100% of asymptotic size (FMNH PR 2123 and UA 8685, respectively). Although preliminary, these results suggest that the 'robust' specimens of *Masiakasaurus* represent full-grown individuals. Of course, further specimens of *Masiakasaurus* require examination (e.g., large 'gracile' specimens and small 'robust' specimens) to confirm that theropod skeletal dimorphism is just a reflection of the two states of maturity (juvenile vs. adult).

ACKNOWLEDGMENTS

We would like to thank members of the Mahajanga Basin Project for their notable field efforts over the past 18 years, and, in particular, for the high-quality excavations at localities MAD 93-18 and MAD 05-42. J. Groenke and V. Heisey provided valuable preparation and molding/casting efforts necessary prior to the completion of this work. R. Hikida and J. Kaufman graciously allowed us to use their respective microscopy equipment. D. W. Krause, M. Carrano, K. Curry Rogers, and N. Myhrvold provided discussions during the early stages of this work. G. Erickson, M. Sander, and H. Woodward provided constructive reviews that improved the presentation and clarity of this paper. Finally, this work was supported by the National Science Foundation (DEB-9224396, EAR-9418816, EAR-9706302, EAR-106477, EAR-116517, EAR-0446488, and EAR-0617561), the National Geographic Society, the Jurassic Foundation, the Ohio University Office of Research and Sponsored Programs, and the Ohio University Heritage College of Osteopathic Medicine.

LITERATURE CITED

Aggrey, S. 2009. Logistic nonlinear mixed effects model for estimating growth parameters. Poultry Science 88:276–280.

Arendt, J. D., and D. N. Reznick. 2005. Evolution of juvenile growth rates in female guppies (*Poecilia reticulata*): predator regime or resource level? Proceedings of the Royal Society of London B 272:333–337.

Azari, R., L. Li, and C. L. Tsai. 2006. Longitudinal data model selection. Computational Statistics and Data Analysis 50:3053–3066.

Bateson, P., D. Barker, T. Clutton-Brock, D. Deb, B. D'Udine, R. A. Foley, P. Gluckman, K. Godfrey, T. Kirkwood, M. M. Lahr, J. McNamara, N. B. Metcalfe, P. Monaghan, H. G. Spencer, and S. E. Sultan. 2004. Developmental plasticity and human health. Nature 430:419–421.

Brisbin, I. L., C. T. Collins, G. C. White, and D. A. McCallum. 1987. A new paradigm for the analysis and interpretation of growth data: the shape of things to come. The Auk 104:552–554.

Bromage, T. G., H. M. Goldman, S. C. McFarlin, J. Warshaw, A. Boyde, and C. M. Riggs. 2003. Circularly polarized light standards for investigations of collagen fiber orientation in bone. Anatomical Record 274B:157–168.

Burnham, K. P., and D. R. Anderson. 2002. Model Selection and Multimodel Inference: A Practical Information-Theoretic Approach, second edition. Springer-Verlag, New York, 488 pp.

Bybee, P. J., A. H. Lee, and E.-T. Lamm. 2006. Sizing the Jurassic theropod dinosaur, *Allosaurus*: assessing growth strategy and evolution of ontogenetic scaling of limbs. Journal of Morphology 267:347–359.

Carrano, M. T., and S. D. Sampson. 2008. The phylogeny of Ceratosauria (Dinosauria: Theropoda). Journal of Systematic Palaeontology 6:183–236.

Carrano, M. T., M. A. Loewen, and J. J. W. Sertich. 2011. New materials of *Masiakasaurus knopfleri* Sampson, Carrano, and Forster, 2001, and implications for the morphology of the Noasauridae (Theropoda: Ceratosauria). Smithsonian Contributions to Paleobiology 95:1–53.

Carrano, M. T., S. D. Sampson, and C. A. Forster. 2002. The osteology of *Masiakasaurus knopfleri*, a small abelisauroid (Dinosauria:

Theropoda) from the Late Cretaceous of Madagascar. Journal of Vertebrate Paleontology 22:510–534.
Castanet, J. 1994. Age estimation and longevity in reptiles. Gerontology 40:174–192.
Castanet, J., S. Croci, F. Aujard, M. Perret, J. Cubo, and E. de Margerie. 2004. Lines of arrested growth in bone and age estimation in a small primate: *Microcebus murinus*. Journal of Zoology 263:31–39.
Chinsamy, A. 1990. Physiological implications of the bone histology of *Syntarsus rhodesiensis* (Saurischia: Theropoda). Palaeontologia africana 27:77–82.
Chinsamy, A. 1993. Bone histology and growth trajectory of the prosauropod dinosaur *Massospondylus carinatus* Owen. Modern Geology 18:319–329.
Cooper, L. N., A. H. Lee, M. L. Taper, and J. R. Horner. 2008. Relative growth rates of predator and prey dinosaurs reflect effects of predation. Proceedings of the Royal Society B 275:2609–2615.
Cormack, D. H. 1987. Ham's Histology. JB Lippincott Co., Philadelphia, 732 pp.
D'Emic, M. D., K. M. Melstrom, and D. R. Eddy. 2012. Paleobiology and geographic range of the large-bodied Cretaceous theropod dinosaur *Acrocanthosaurus atokensis*. Palaeogeography, Palaeoclimatology, Palaeoecology 333–334:13–23.
Dennis, B., and M. L. Taper. 1994. Density dependence in time series observations of natural populations: estimation and testing. Ecological Monographs 64:205–224.
Enlow, D. H. 1963. Principles of Bone Remodeling. An Account of Postnatal Growth and Remodeling Processes in Long Bones and the Mandible. Charles C. Thomas, Springfield, Illinois, 131 pp.
Erickson, G. M., and T. A. Tumanova. 2000. Growth curve of *Psittacosaurus mongoliensis* Osborn (Ceratopsia: Psittacosauridae) inferred from long bone histology. Zoological Journal of the Linnean Society 130:551–566.
Erickson, G. M., K. Curry-Rogers, and S. A. Yerby. 2001. Dinosaurian growth patterns and rapid avian growth rates. Nature 412:429–433.
Erickson, G. M., P. J. Makovicky, P. J. Currie, M. A. Norell, S. A. Yerby, and C. A. Brochu. 2004. Gigantism and comparative life-history parameters of tyrannosaurid dinosaurs. Nature 430:772–775.
Erickson, G. M., O. W. M. Rauhut, Z. Zhou, A. H. Turner, B. D. Inouye, D. Hu, and M. A. Norell. 2009. Was dinosaurian physiology inherited by birds? Reconciling slow growth in *Archaeopteryx*. PLoS ONE 4:e7390.
Frylestam, B., and T. Schantz. 1977. Age determination of European hares based on periosteal growth lines. Mammal Review 7:151–154.
Gaillard, J.-M., D. Pontier, D. Allaine, A. Loison, J.-C. Herve, and A. Heizmann. 1997. Variation in growth form and precocity at birth in eutherian mammals. Proceedings of the Royal Society of London B 264:859–868.
Hemelaar, A. S. M., and J. J. Van Gelder. 1980. Annual growth rings in phalanges of *Bufo bufo* (Anura, Amphibia) from the Netherlands and their use for age determination. Netherlands Journal of Zoology 30:129–135.
Horner, J. R., and K. Padian. 2004. Age and growth dynamics of *Tyrannosaurus rex*. Proceedings of the Royal Society of London B 271:1875–1880.
Horner, J. R., A. J. deRicqlès, and K. Padian. 1999. Variation in dinosaur skeletochronology indicators: implications for age assessment and physiology. Paleobiology 25:295–304.
Hübner, T. R. 2012. Bone histology in *Dysalotosaurus lettowvorbecki* (Ornithischia: Iguanodontia)—variation, growth, and implications. PLoS ONE 7:e29958.
Hurvich, C. M., and C.-L. Tsai. 1989. Regression and time series model selection in small samples. Biometrika 76:297–307.
Hutton, J. M. 1986. Age determination of living Nile crocodiles from the cortical stratification of bone. Copeia 1986:332–341.
Klein, N., and P. M. Sander. 2007. Bone histology and growth of the prosauropod dinosaur *Plateosaurus engelhardti* von Meyer, 1837 from the Norian bonebeds of Trossingen (Germany) and Frick (Switzerland). Special Papers in Palaeontology 77:169–206.
Köhler, M., and S. Moyà-Solà. 2009. Physiological and life history strategies of a fossil large mammal in a resource-limited environment. Proceedings of the National Academy of Sciences of the United States of America 106:20354–20358.
Köhler, M., N. Marin-Moratalla, X. Jordana, and R. Aanes. 2012. Seasonal bone growth and physiology in endotherms shed light on dinosaur physiology. Nature 487:358–361.
Lance, V. A. 2003. Alligator physiology and life history: the importance of temperature. Experimental Gerontology 38:801–805.
Lee, A. H. 2004. Histological organization and its relationship to function in the femur of *Alligator mississippiensis*. Journal of Anatomy 204:197–207.
Lee, A. H., and S. Werning. 2008. Sexual maturity in growing dinosaurs does not fit reptilian growth models. Proceedings of the National Academy of Sciences of the United States of America 105:582–587.
Lee, A. H., A. K. Huttenlocker, K. Padian, and H. N. Woodward. 2013. Analysis of growth rates; pp. 217–251 in K. Padian and E.-T. Lamm (eds.), Bone Histology of Fossil Tetrapods: Advancing Methods, Analysis, and Interpretation. University of California Press, Berkeley, California.
Lehman, T. M., and H. N. Woodward. 2008. Modeling growth rates for sauropod dinosaurs. Paleobiology 34:264–281.
Lindstrom, M. J., and D. M. Bates. 1988. Newton-Raphson and EM algorithms for linear mixed-effects models for repeated-measures data. Journal of the American Statistical Association 1014–1022.
de Margerie, E., J. Cubo, and J. Castanet. 2002. Bone typology and growth rates: testing and quantifying 'Amprino's rule' in the mallard (*Anas platyrhynchos*). Comptes Rendus Biologies 325:221–230.
Morris, P. 1970. A method for determining absolute age in the hedgehog. Journal of Zoology 161:277–281.
Padian, K., J. R. Horner, and A. de Ricqlès. 2004. Growth in small dinosaurs and pterosaurs: the evolution of archosaurian growth strategies. Journal of Vertebrate Paleontology 24:555–571.
R Development Team. 2011. R: A Language and Environment for Statistical Computing. R Foundation for Statistical Computing, Vienna, Austria.
Richards, F. J. 1959. A flexible growth function for empirical use. Journal of Experimental Botany 10:290–300.
de Ricqlès, A. J., J. Castanet, and H. Francillon-Vieillot. 2004. The "message" of bone tissue in paleoherpetology. Italian Journal of Zoology, Supplement 1:3–12.
de Ricqlès, A. J., K. Padian, and J. R. Horner. 2003. On the bone histology of some Triassic pseudosuchian archosaurs and related taxa. Annales de Paleontologie 89:67–101.
Roberts, E. D., C. L. Matlock, T. Joanen, L. McNease, and M. Bowen. 1988. Bone morphometrics and tetracycline marking patterns in young growing American alligators (*Alligator mississippiensis*). Journal of Wildlife Diseases 24:67–70.
Rogers, R. R., D. W. Krause, K. C. Rogers, A. H. Rasoamiaramanana, and L. Rahantarisoa. 2007. Paleoenvironment and paleoecology of *Majungasaurus crenatissimus* (Theropoda: Abelisauridae) from the Late Cretaceous of Madagascar. Journal of Vertebrate Paleontology 27:21–31.
Rootes, W. L., R. H. Chabreck, V. L. Wright, B. W. Brown, and T. J. Hess. 1991. Growth rates of American alligators in estuarine and palustrine wetlands in Louisiana. Estuaries 14:489–494.
Sampson, S. D., M. T. Carrano, and C. A. Forster. 2001. A bizarre predatory dinosaur from the Late Cretaceous of Madagascar. Nature 409:504–506.
Sander, P. M., and P. Andrassy. 2006. Lines of arrested growth and long bone histology in Pleistocene large mammals from Germany: what do they tell us about dinosaur physiology? Palaeontographica, Abteilung A 277:143–159.
Sander, P. M., and N. Klein. 2005. Developmental plasticity in the life history of a prosauropod dinosaur. Science 310:1800–1802.
Sander, P. M., O. Mateus, T. Laven, and N. Knötschke. 2006. Bone histology indicates insular dwarfism in a new Late Jurassic sauropod dinosaur. Nature 441:739–741.
Sebens, K. P. 1987. The ecology of indeterminate growth in animals. Annual Review of Ecology and Systematics 18:371–407.
Tsuihiji, T., M. Watabe, K. Tsogtbaatar, T. Tsubamoto, R. Barsbold, S. Suzuki, A. H. Lee, R. C. Ridgely, Y. Kawahara, and L. M. Witmer. 2011. Cranial osteology of a juvenile specimen of *Tarbosaurus bataar* (Theropoda, Tyrannosauridae) from the Nemegt Formation (Upper Cretaceous) of Bugin Tsav, Mongolia. Journal of Vertebrate Paleontology 31:497–517.
Turvey, S. T., O. R. Green, and R. N. Holdaway. 2005. Cortical growth marks reveal extended juvenile development in New Zealand moa. Nature 435:940–943.
Tykoski, R. S., and T. Rowe. 2004. Ceratosauria; pp. 47–70 in D. B. Weishampel, P. Dodson, and H. Osmólska (eds.), The Dinosauria, Second Edition. University of California Press, Berkeley, California.

Varricchio, D. J. 1993. Bone microstructure of the Upper Cretaceous theropod dinosaur *Troodon formosus*. Journal of Vertebrate Paleontology 13:99–104.

Vonesh, E. F., and R. L. Carter. 1992. Mixed-effects nonlinear regression for unbalanced repeated measures. Biometrics 48:1–17.

Woodward, H. N., J. R. Horner, and J. O. Farlow. 2011. Osteohistological evidence for determinate growth in the American alligator. Journal of Herpetology 45:339–342.

Xu, X., Q. Tan, J. Wang, X. Zhao, and L. Tan. 2007. A gigantic bird-like dinosaur from the Late Cretaceous of China. Nature 447:844–847.

Xu, X., J. M. Clark, C. A. Forster, M. A. Norell, G. M. Erickson, D. A. Eberth, C. Jia, and Q. Zhao. 2006. A basal tyrannosauroid dinosaur from the Late Jurassic of China. Nature 439:715–718.

Xu, X., J. M. Clark, J. Mo, J. Choiniere, C. A. Forster, G. M. Erickson, D. W. E. Hone, C. Sullivan, D. A. Eberth, S. Nesbitt, Q. Zhao, R. Hernandez, C. Jia, F. Han, and Y. Guo. 2009. A Jurassic ceratosaur from China helps clarify avian digital homologies. Nature 459:940–944.

Yates, A. 2005. A new theropod dinosaur from the Early Jurassic of South Africa and its implications for the early evolution of theropods. Palaeontologia africana 41:105–122.

Zullinger, E. M., R. E. Ricklefs, K. H. Redford, and G. M. Mace. 1984. Fitting sigmoidal equations to mammalian growth curves. Journal of Mammalogy 65:607–636.

Submitted May 22, 2012; revisions received September 29, 2012;
accepted October 16, 2012.
Handling editor: Emily Rayfield.